Physics of Earth

Funtikov A.I. Phase diagram and melting curve results of iron and iron-nickel alloy of shock-wave and static measurements in the earth's core states

Institute of thermophysics of extreme states RAS, Moscow
funtikov@hedric.msk.su

Previous shock-wave measurement results of compressibility, sound speed and temperatures on adiabats of impact compression of iron and iron- nickel alloys in the range of pressure from 140 up to 350 GPa were used for calculations of distribution of density and temperature in the Earth's core and examinations of the appropriate model submissions. One of the main directions here consists in the determination of melting curve of iron and temperature of outer liquid and inner solid core boundary, at pressure 330 GPa. The Earth's core consitsts mainly of iron, but there are nickel and light elements in the outer core, that may decrease melting temperature in this range states.

In the last years in connection with significant static technical measurement developments of diamond anvil cell with laser heating of sample pressure range was essentially extended (up to 200 GPa) and temperatures in the range of melting curve for iron that allowed to define the phase diagrams and to extrapolate this data to the conditions, achieved by shock compression.

Despite some inside disagreement of experimental data sets of static and shock-wave measurements, there is the essential divergence between these results, apparently, lying outside observed errors of both sets of experiments, that caused various positions of the determined by these methods melting curve on the phase diagram and accordingly to various temperature estimates of the internal region of the Earth [1]. So, on measurements of sound speed on shock adiabat [2] the melting on it answers pressure P = 240 GPa and temperature T = 5700 K, but intersection of static melting curve [3] with shock adiabat - P = 155 GPa and T = 3600 K. The shock-wave data of iron-nickel alloy agree with the similar data on iron, as a whole, allow to expand the compare analysis of experimental data sets with the results of static measurements. Some distinction of shock compression data at higher pressure for the γ-phase alloy and iron is connected to α→ε phase transition in it at pressure 13 GPa.

To consider the above contradictions we carried out some additional experimental determination of the parameters of shock compression of iron and iron-nickel alloy (stainless steel) corresponding to the melting at normal pressure for want of expansion after shock compression [4]. The used method is based on the establishment of attributes of melting in the subjected to loading samples. The shock-wave pressure was determined to be 140 and 175 GPa. Such data corresponding to the lower boundary of melting curve, can be used for reliable estimate of temperature relation on isentope by the results of shock-wave experiment [5], and also for examination of adequacy of calculations on the equations of states of the phase diagram and melting curve. At the same time, taking account of high reliability of static measurement results at initial pressure, these data also allow to extrapolate melting curve to higher pressures.

For the initial point of these estimates of the curve melting of iron and alloy [6] the triple point of interception of γ-ε phase boundary and melting curve of iron is accepted determined on more accurate static measurements [3] at P = 60 GPa, T = 2800 K. This point answers also the data of static measurements of melting curve [7] and extrapolated γ-ε phase boundary [8] of iron-nickel alloy.

Using these data in γ-phase range of iron and alloy, the appropriate isothermal compressibility data and Lindemann low of melting curve, Gruneisen ratio from density, and from them isentope position, corresponding melting at normal pressure were determined . Incidentally discontinuty isentrope on phase boundary in γ-phase range was taken into account .

Thus the isentrope states in the ε-phase range becomes known in two points - on γ-ε phase boundary and on the shock adiabat. Both points correspond to rather small density change from 9.5 up to 11.5 g cm^{-3}. Assuming, as well as earlier for γ-phase range, that the Gruneisen ratio is inversely proportional to density, it was determined, an then melting curves were obtained using Lindemann low. In the range of pressure ~ 150 GPa the melting curve of iron-nickel alloy appeared below (~100 K) the appropriate curve for iron.

The melting curves for both materials, obtained from the isentrope expansions data, passing through the common triple point, appeared to be close enough to the melting curve of iron [3], though a little bit above it at P = 150 GPa, on 100-200 K. Obtained results for iron and alloy answer lower values of melting curve temperatures and do not eliminate the indicated contradiction between the groups of static and dynamic measurements, though the recent results [9, 10] show these data to be somewhat closer.

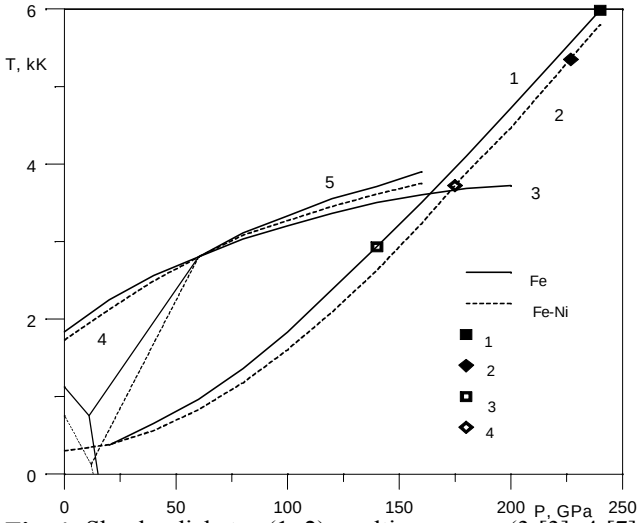

Fig. 1. Shock adiabates (1, 2), melting curves (3 [3], 4 [7] and 5 - present work) and phase boundares for iron and

iron-nickel alloy; shock-wave measurements for the melting (1, 2) and isentope (3, 4).

References:

1. Boehier R. // Annu. Rev. Earth Planet Sci. 1996. V. 24. P. 15-40.
2. Brown J.M., McQueen R.G. // J. Geophys. Res. 1986. V. 91. P. 7485-7494.
3. Shen G. et al. // Geophys. Res. Lett. 1998. V. 25. N 3. P. 373-376.
4. Funtikov A.I., Osipov R.S., Tsyganov V.A. // High Temper. 1999. V. 37. N 6. P. 887-894.
5. Zel'dovich Ya.B. // Zh. Eks. Teor. Fiz. 1957. T. 32. № 6. C. 1577-1578.
6. Funtikov A.I. // Izv. RAN, Ser. Fiz. Zemli. 2000 (in the press).
7. Couty R. et al. // High Pressure Science and Technology-1995. AIPAPT, 1995. P. 314-316.
8. Huang E. et al. // J. Geophys. Res. 1992. V. 97. P. 4497-4502.
9. Nguyen J.H., Holms N.C. // High Pressure Science and Technology-1999. AIPAPT, 1999. P. 156-159.
10. Anderson O.L., Duba Al // J. Geophys. Res. 1997. V. 101. N 10. P. 22659-22669.

Avsyuk Yu.N., Svetlosanova Z.P. Why does the moon's equation coinside with the plane of ecliptic ?

The United Institute of Physics of the Earth RAS, B.Grusinskaya 10, Moscow 123810 avsyuk@uipe-ras.scgis.ru

key words [*seismic activity tidal influence Earth Sun perturbations orbital movement stages of formation figure of the Moon*]

The investigation of the tidal constitutes is a field of celestial mechanics of the bodies, which have geometrical sizes. The sequence of investigation of the tidal forces is similar to the sequence of investigation of the orbital movement, which is accepted in celestial mechanics. As the first approximation is given the description of tidal force in the case of unperturbed (Keplerian) movement of the investigated and the external body (the problem of two bodies). Then is given the description of the tidal force in the case of the perturbed, corresponding to the actual materials of observation, orbital movement of the investigated body (the problem of n-bodies).

I. Newton gave in geometrical figures the full description of the tidal force, i.e. the parts, corresponding to keplerian movement, plus perturbations [1]. P.S. Laplace gave in analytical form the description of tidal force only in the case of unperturbed (keplerian) movement of the investigated and the external body (the problem of two bodies).

In modern science the formula of Laplas is used, which characterizes the tidal force in pairs:the Earth–the Moon, the Earth–the Sun, the Earth–the Venus or the Moon–the Earth, the Moon–the Sun, the Moon–the Jupiter and so on.

The summary of tidal forces, corresponding to pair interactions, gives an incomplete description of power influence. It is impermissible especially in the case of tidal processes on the Moon, where the unperturbed part of the influence of the Moon and the Sun is estimated as $1{,}2\cdot10^{-3}$ cm/s^2 and $0{,}7\cdot10^{-5}$ cm/s^2 and the perturbed part has a greater module, which is equal to $1{,}5\cdot10^{-3}$ cm/s^2. That's why the comparison of the Moon's seismic activity with the variations of tidal influence with the Earth and the Sun on the Moon, which were calculated using the formula of Laplace, didn't illuminate their interconnection. After the addition (according to I. Newton) of the perturbations, produced by the Sun, to the description of tidal force the cause–effect connection of tidal influence with the manifestation of the activity of deep (800–1000 km) and nearsurface (25–300 km) centers is estimated convincingly enough.

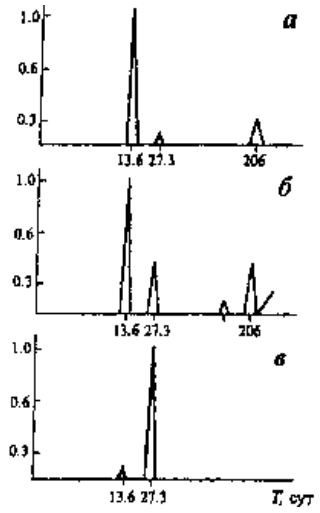

Period, days

Fig. 1 [2,3,4]. The comparison of spectra at the main tidal waves, calculated using the formula of Laplas (*в*), or using formula of Newton (*а*) with the spectrum of repeated moonquakes, registered during the experiment «Apollo» (21.04.72-21.05.74) (*б*).

Periodically changing tidal force on a geological scale of time (hundred of millions of years) may be considered as «vibration». That's why the figure of celestial body, which is formed by axial rotation, bears an imprint of the direction of an acting «vibration». The dominating harmonics of tidal force are linked to the plane of ecliptic, where the value of perturbation, produced by the Sun, is maximal. Consequently, the tendency of formation of the Moon's figure had the preferable direction.

In favor of originally fast axial rotation of the Moon and tidal warming of the Moon's internal regions at the first stages of formation of the system the Earth–the Moon advocates a substantial magnetic field with the age of 4,0–3,7 milliards of years. Mechanical warming (i.e. thermal losses, corresponding to cyclic deformations) favored the beginning of inhibition of the Moon's axial rotation and the transition of the Moon to the nearly synchronic state of rotation at the approximately 3 mlrd. years, as can be judged by the fall of magnetic value from 0,3 to 0,05 oersted. During the period from 4,0 to 3,0 mlrd. years the Moon has significantly lost the angular speed of rotation and in the course of cooling, which has begun (volcanic activity finished at 3,3 mlrd. years ago),the modern figure of Moon has formed. As the Moon's equator lies in the plane of ecliptic, the figure has formed under the

condition: the Sun's influence is greater than the Earth's. The shift of 3 km of the Moon's center of mass relative to its geometrical center towards the Earth, as well as basaltic effluxes only on the Moon's surface, which is visible from the Earth, indirectly favor the shift of molten masses under the influence of perturbed parts of tidal influence of the Sun on the Moon.

The lack of folded mountains on the Moon points to, most probably, the fact that the powerful influence of the Sun at the period 4,0 to 3,0 mlrd. years has completely formed and oriented the figure of the Moon in the plane of ecliptic, and the influence of the Earth made no subsequent correction.

All these reconstructions, surely, are open to discussion. But it is clear that the early stages of the evolution could take part at a substantial withdrawal of the Moon from the Earth, exceeding the modern size of the orbit. That's why during the original stages the tidal influence dominated on internal regions, and the change of their aggregate condition caused the loss of axial rotation and the gradual declination of the power of mechanical warming. The Moons example clearly demonstrates that traditional, settled recommendations how to calculate the tidal force must be carefully analyzed within the framework of dynamics, and that one should not use statical analogies, which seem to be clear.

References:

1. Avsyuk Yu.N. On the tidal influence // Pis'ma v AZh 1977, V.3, №4, pp.184-188.
2. Lammlein D.R. Lunar seismicity and Tectonics. // Physics of the Earth and Planetary Interiors, 1977, 14, 224-273.
3. Galkin I.N. Geophysics of the Moon.// M., Nauka, 1987, 174 p.
4. Avsyuk Yu.N. Perturbation members in tidal influence on the Moon for comparison with the Moon's seismic activity./ Preprint №8, AN SSSR, IPhZ im. O.Yu. Schmidta, M., 1981, 25 p.

#Kronrod V.A. and Kuskov O.L. Assessment of chemical composition of the continental upper mantle of the Earth

Vernadsky Institute of Geochemistry and Analytical Chemistry
ol_kuskov@mail.ru

key words: [*Earth, mantle, composition*]

Thermodynamic approach and method of calculation. For computation of the seismic velocity profiles in the Earth's mantle (direct problem), we need a chemical model and a model for the temperature distribution. Since composition of the entire mantle is uncertain, it will take a great variety of input compositions. Another approach involves the computation of the geophysically admissible bulk composition and density distribution models in the mantle layers (inverse problem). Thermodynamic modeling of the phase relations and physical properties of the multicomponent mineral system at high pressures and temperatures was used to develop a method for solving the inverse problem of determining the bulk composition, density and temperature distribution in the continental upper mantle of the Earth from the totality of geophysical evidence [1]. The goal of the inversion procedure is to find a self-consistent petrological-geophysical model that minimises the discrepancies between the calculated parameters and "reference model". The determination of bulk composition from the seismic data generally can have many solutions. To choose the best one from a range of solutions, we should impose some extra conditions, for example, a close agreement of the temperature and bulk composition derived from the solution of the inverse problem with the parameters for a "reference model". For this purpose, we have used the following conditions.

The temperature distribution in the mantle has been modelled by the continental geotherm [2]. Seismic velocity profiles as a function of depth have been taken from the recent seismic model IASP 91 [3]. Chemical composition of the continental upper mantle at depths of 50-400 km has been modelled by the average composition of the spinel and garnet peridotites [4-6]. The chemical and phase compositions of the mantle were modelled within the system CaO-FeO-MgO-Al_2O_3-SiO_2 (CFMAS) including the pure phases and solid solutions: olivine, spinel, garnet (almandine, grossular, pyrope); orthopyroxene and clinopyroxene (5-component solutions). The observed and calculated values of the thermophysical properties were correlated with the THERMOSEISM software [3]. The package contains thermodynamic databases and subroutines for calculating mineral equilibria at high pressures and temperatures by the method of the minimisation of the total Gibbs free energy. It can be used to calculate the equilibrium mineral composition of a multicomponent system, compute the physical properties of a mineral assemblage (including the densities and seismic velocities), and obtain the petrological and geophysical constraints on the bulk chemical composition of a planetary body. Typical errors in calculating the mantle density are better than 1%.

The solution of the inverse problem is based on the minimisation of the function [7]:

$$\vartheta = \sum_{i=1}^{N} \sum_{F} \alpha_F \left(F_i^0 - F_i\right)^2,$$

($F=V_p, V_s, T, C_m$), (m=FeO, MgO, Al_2O_3, CaO),
where F_i^o are the parameters of the "reference model", N is the number of points along the depth. C(FeO, MgO, Al_2O_3, CaO) are the oxide concentrations; the concentration of SiO_2 is determined from normalisation. With proper selection of the weight coefficients α_F, the influence of the F function on the solution can be adjusted, and the solution can be made to meet extra conditions. In making inverse problem, we require a non-negative density gradient in the mantle ($d\rho/dH > 0$) and assume using the arguments on $C_{Al_2O_3}/C_{CaO}$ ratios and ratio's increments $\delta C_{Al_2O_3}/\delta C_{CaO}$ in the mantle [4] that $\delta C_{Al2O3} = BC\delta_{MgO}$, $C_{CaO} = KC_{Al2O3}$ ($B < 0$). We have obtained that B=-0.325, K=0.97 (H=70-80 км); B=-0.325, K=0.7+0.0018(H(км)-120) (H=90-210 km); B=-0.5, K=0.8 (H=220-400 км).

*Results and Discussion***.** Chemical composition of the continental upper mantle, seismic velocities, temperature and density distribution based on minimising deviations of the calculated values of seismic velocities, concentrations,

This study was partly supported by the Russian Foundation for Basic Research (project 00-05-64371).

and temperature from corresponding seismic, petrological, and thermal data are shown in Table 1. The calculated temperatures and velocity profiles are within the reasonable limits of all uncertainties involved in geophysical observations [2, 3]. The results of calculation show the radial compositional variations in the upper mantle.

Table 1. The calculated chemical composition (wt.%) and physical properties of the continental upper mantle

H_{km}	T^oC	C_{MgO}	C_{FeO}	C_{Al2O3}	C_{CaO}	C_{SiO2}	V_p^o	V_p	V_s^o	V_s	ρ	Mg#
71	841	41.5	8.20	1.95	1.90	46.45	8.04	8.05	4.48	4.56	3.295	.900
120	1120	43.5	8.10	1.20	.84	46.36	8.05	8.12	4.50	4.54	3.295	.905
171	1329	43.3	7.90	1.27	1.02	46.51	8.19	8.20	4.51	4.53	3.317	.907
210	1400	43.2	7.90	1.29	1.12	46.49	8.30	8.30	4.52	4.55	3.346	.907
271	1434	42.7	8.35	2.20	2.13	44.62	8.52	8.52	4.63	4.62	3.42 0	.901
371	1491	40.0	8.37	3.50	2.80	45.33	8.89	8.80	4.80	4.72	3.530	.895
400	1508	38.0	8.40	4.50	3.60	45.50	9.03	8.89	4.87	4.76	3.560	.890

V_p^o and V_s^o are from [3].

Table 2. Bulk composition models (wt.%) of the continental upper mantle

Oxides	H≤70 км	70<H≤210 км	H > 230 км
SiO_2	≅46	≅46 ($<(C_{SiO2})_{70}$	44.5-45.5
Al_2O_3	≅2	1.2-1.3	≥ 2.0
FeO	≅8	≅8 ($<(C_{FeO})_{70}$	8.3-8.5
MgO	≅41	>43	38.0-42.7
CaO	≅1.9	0.8-1.2	≥ 2.0

The average bulk composition model of the upper mantle is presented in Table. 2. According to the calculated chemical composition, the continental upper mantle may consist of: spinel peridotites at depths of < 70-80 km, low-temperature peridotites at depths of 80-210 km, and high-temperature peridotites at depths of > 210-230 km. Our analysis of the composition of the upper mantle leads to the conclusion that the upper mantle of the Earth may consist of two regions with a chemical boundary at depths of 210-230 km. Such a model gives the best fit to the mantle seismic properties. It should be emphasised that the derived composition is model-independent in geochemical context but the degree of its reliability is almost completely defined by the accuracy of seismic and thermal data.

References:

1. Kronrod V.A., Kuskov O.L., 1996. Determination of temperature and bulk composition of the upper mantle from seismic data. *Geochem. Intern.,* 34: 72-76.
2. Pollack H.N., Hurter J., Johnson R., 1993. Heat flow from the Earth's interior: analysis of the global data set. *Rev. Geophys.,* 31: 267-280.
3. Kennet B.L.N., Engdahl E.R., 1991. Travel times for global earthquake location and phase identification. *Geophys. J. Int*., 105: 429-465.
4. McDonough W.F., 1990. Constrains on the composition of the continental lithospheric mantle. *Earth Planet. Sci. Lett.,* 101: 1-18.
5. Maaloe S., Aoki K.I., 1975. The major element composition of the upper mantle estimated from the composition of lherzolites. Contrib. Mineral. Petrol., 63: 161-173.
6. Ilupin I.P., 1989. Chemical composition of xenoliths from kimberlites. Geochemistry of the deep interior of the Earth. Ed. B.G.Luts. Moscow, Inst. Fiziki Zemli, 26-68.
7. Kuskov O.L., Kronrod V.A., 1998. Constitution of the Moon: 5. Constraints on composition, density, temperature, and radius of a core. Phys. Earth Planet. Inter., 107: 285-306.

Sharikov I.O. Origin of a lunar regolith. Simulation research

A.A.Baikov Institute of Metallurgy and Material Research Russian Academy of Sciences intercon@ultra.imet.ac.ru

As known, the surface layers of moon are formed at the expense of bombardment with meteorites, sedimentation of ejections and partial condensation of particles. A major factor of its formation is the specific power of energy release. It can vary over a wide range, depending on a velocity and mass of bombarded particles. The velocity of particles is from 3 to 70 km/s, mass of meteorites is 10^{-10}-10^{10} g.

Thus, the formed surface layer of moon is regolith. This is a mixture of the solid particles of ejections formed due to the meteoritic impacts, the solidified drops and a condensate of a vapor phase.

The purpose of the present work was to study morphology and structure of a condensate. This condensate was formed during a shock destruction of basalt with the laser pulses. This process simulated a meteoritic effect.

The main attention in this article was given to the study of a condensate under relatively low powers of the specific energy releases (up to 10^8 W/cm^2). These values of power correspond to velocities of meteorites or their secondary splinters close to 2.4 km/s.

The micrometeoritic effect was simulated with the pulsed laser effect. The criterion of energy release both of meteoritic impact and pulse laser effect was in a basis of simulation. In the present work the usual volcanic rock,

i.e. basalt, was selected as investigated sample. The surface of the basalt was carefully polished and subjected to irradiation of the pulse laser. The laser irradiation wavelength was equal to 1.06 microns, energy of pulse was equal to 100 J. Power density varied within the range from 10^6 to 10^7 W/cm^2, pulse duration was ~ 10^{-3} s. The sample was fixed inside the special chamber, with vacuum ~ 10^{-5} torr. The polished silicon plates and the aluminium foils were used for the collection of a condensate and scattering products of laser impulse effect. The thickness of a condensate layer was approximately 0.1 mm for want of repeated (some tens impulses) exposure of various sites of the basalt target.

It has been shown, that the morphology of a condensate surface in these simulation investigations partially corresponds to real morphology of a moon surface rock. Both the spherical particles and the particles of an irregular form were formed. Besides the typical form shrinkholes was observed on the surface. It depends on the conditions of condensation of liquid ejected droples. As considered earlier, that it is a result of a micrometeoritic effect.

Didenko A. and Tikhonov L. Magnetic petrology of cenozoic basalts in Central Asia

Schmidt United Institute of Physics of the Earth, Russian Academy of Sciences B.Gruzinskaya 10 Moscow 123810 Russia
didenko@uipe-ras.scgis.ru

The hotspot hypothesis proposed by Morgan [1972] provides a deeper insight into many processes in the Earth as well as into their interrelations. The hotspots are surface evidence of ascending convective mantle flows. Usually they coincide with areas of recent or ancient triple junctions of diverging plate boundaries. Most of the typical hotspots (Hawaii, Reunion, Samoa, Iceland, Bouvet) are located on the surface of the oceanic lithosphere. The hotspots recognized within the continental lithosphere are few, and one of the most studied is the Afar triangle at the triple junction of the Sheba Range, Ethiopian rift, and Assal rift [Shilling et al., 1992].

Grachev [1998] believes that the number of hotspots is actually much greater and theoretically must coincide with the number of triple junctions existing in the lithosphere; they need a detailed isotope-geochemistry analysis. In this respect, of great interest is Central Asia with its widespread intraplate basaltic volcanism. The hotspot (or hotspots) located on the territory of the trans-Baikal region and Mongolia a is unique one because an intense magnetic anomaly is present there.

Two spatially separate areas of Cenozoic volcanism exist on this territory: (1) a zone trending nearly N-E and extending from the Baikal rift zone in the north to the trans-Altai Gobi in the south and (2) the vast Dariganga plateau in southeastern Mongolia with a small area in the Halhin-Gol River basin [Grachev, 1998; Saltykovsky and Genshaft, 1985]. Geomorphological and stratigraphic evidence and absolute datings of basalts suggest that an E-W magmatic zone existed in Mongolia (present-day coordinates) in the Cenozoic and migrated north-northeast, with the Pliocene-Quaternary volcanism being localized within the Khamar Daban and Hangai Ranges and the Dariganga plateau [Continental volcanism ..., 1983].

The Cenozoic volcanic rocks of Mongolia are represented solely by basaltic varieties dominated by rocks that are strongly depleted in silica. Tholeiitic varieties with more than 5%-7% of normative hypersthene are rather widespread and compose most of the Pliocene sheets and extended flows that is likely associated with fissure eruptions. However, according to classification schemes based on the SiO_2-(Na_2O+K_2O), nearly all of the basaltoids under consideration belong to alkaline and subalkaline varieties. The volcanites are primarily alkali-olivine basalts (mostly of the Na-K type), which defines their petrochemical properties. They are characterized by low concentrations of silica and alumina and by high Ti and P concentrations.

Table. Petrochemical characteristics of basalts

T_C,°C	J_n, A/m	$\kappa\times10^2$, SI units	Q_n	J_s, A m^2/kg	J_{rs}/J_s	H_{cr},mT	J_{st}/J_{s0}
150	13.2	2.8	19.4	1.4	0.13	13.1	1.17
230	17.6	1.8	44.6	1.1	0.13	15.5	1.54
350	4.7	1.0	8.1	0.8	0.15	28.7	0.97
560	16.4	2.6	14.9	2.2	0.17	37.7	0.90

Note: The notation is as follows: T_C, Curie point; J_n, NRM; κ, initial magnetic susceptibility; Q_n, Koenigsberger factor; J_s, saturation magnetization; H_{cr}, remanent coercivity; J_{s0} and J_{st}, saturation magnetizations before and after laboratory heating to 650°C, respectively.

Over 70 samples from the collections of Yu.S. Genshaft and A.F. Grachev were taken for the petromagnetic examination which included measurement and analysis of such standard characteristics as the magnetic susceptibility, natural remanent magnetization (NRM), Koenigsberger ratio, remanent destructive field, saturation magnetization and its remanent value. Petromagnetic analysis was conducted to study the magnetic mineralogy of the basalts: the J_s-T and J_{rs}-T relations were examined and used for the determination of Curie points.

The preheating magnetic parameters of the studied samples virtually coincide with similar characteristics of the majority of both oceanic and continental basalts, thereby implying a general mechanism that controlled the formation of their ferromagnetic fraction, although there are some divergences in ferromagnet concentrations. In the collection studied, the latter are 1.5 to 2 times as high as in oceanic basalts.

The thermomagnetic analysis showed that the Curie points, determining the ferromagnetic fraction composition, vary within wide limits (from 140° to 600°C), ranging from titanomagnetites to weakly oxidized

magnetite. Some of the titanomagnetites are likely to have been altered as a result of the secondary oxidation, which increased their Curie points. However, no continuous alteration of the ferromagnetic fraction is observed. The resulting histograms showed the presence of four modal T_C values of about 150, 230, 350 and 560°C (Table). Grouping the petromagnetic characteristics in accordance with the modal T_C values (the magnetite phase is ignored because it is a product of the primary titanomagnetite decomposition), the following regular pattern is observed: an increase in the extent of titanomagnetite oxidation decreases the magnetic susceptibility (from 0.028 to 0.01 SI units) and saturation magnetization (from 1.4 to 0.8 A m^2/kg) and results in a more than twofold increase in the remanent coercivity (from 13.1 to 28.7 mT).

Such correlations (negative, between T_C and J_s, and positive, between T_C and H_{cr}) are characteristic of basalts subjected to oxidation, when fragmentation of the effective magnetic volume into several domains increases the magnetic hardness and decreases the volume concentration of magnetization carriers in rock. It remains unclear whether the 230 and 350°C Curie points are oxidized or initial values. The primary nature of the titanomagnetites with Curie points of about 150, 230 and 350°C is supported by the discreteness of their distribution, and a model of melt formation at different depths may be suggested as an alternative to the oxidation variant. The basalts with 150°C Curie points were derived from melts that formed at the deepest depth level, and the 230°C basalts, from shallower melts.

Such a mechanism was already proposed by Didenko et al. [1999] for the formation of hotspot basalts at the Bouvet triple junction: as well as in central Mongolia, a bimodal distribution of Curie points of basalts (120-140°C and 210-240°C) and their positive correlation with magnetic hardness parameters are observed there. In this case, a higher magnetic hardness appears to be related to the defects acquired by magnetic grains at the stage of their crystallization.

We are grateful to Yu.S. Genshaft, A.F. Grachev, G.N. Petrova, and D.M. Pechersky for discussion and helpful comments. This work was supported by the Russian Foundation for Basic Research, project no. 99-05-64000.

References:

1. Continental Volcanism in Mongolia, Moscow: Nauka, 1983, 189 p.
2. Didenko, A.N., et al., Petromagnetic and petrological variations along the Mid-Atlantic and Southwestern Indian ridges in the Bouvet triple junction region, Fiz. Zemli, 1999, no. 12, pp. 47-66.
3. Genshaft, Yu.S. and Saltykovsky, A.Ya., A Catalog of Inclusions of Deep Rocks and Minerals in Mongolia Basalts, Moscow: Nauka, 1990, 72 p.
4. Grachev, A.F., The Khamar Daban Range as a hotspot of the Baikal rift: Evidence from chemical geodynamics, Fiz. Zemli, 1998, no. 3, pp. 3-28.
5. Morgan, W.J., Deep mantle convection plumes and plate motions, Am. Assoc. Petroleum Geologist Bull., 1972, vol. 56, pp. 203-213.
6. Saltykovsky, A.Ya. and Genshaft, Yu.S., Geodynamics of the Cenozoic Volcanism in Southwestern Mongolia, Moscow: Nauka, 1985, 136 p.
7. Shilling, J.G., et al., Nd-Sr-Pb isotopic variations along the Gulf of Aden: evidence for Afar mantle plume-continental lithosphere interaction, J. Geophys. Res., 1992, vol. 97, no. B7, pp. 10927-10966.

#Basilevsky A.T.[1], Yakovlev O.I.[1], Fisenko A.V.[1], Semjonova L.F.[1], Moroz L.V.[2], Pieters C.M.[3], Hiroi T.[3], Zinovieva N.G.[4], Keller H.U.[5], Semenova A.S.[1], Barsukova L.D.[1], Roshchina I.A.[1], Galuzinskaya A.Kh.[1], Stroganov I.A.[1] Simulation of effect of impact melting on optical properties of martian soil.

[1]Vernadsky Institute, Moscow, *Russia*,
[2]DLR Institute for Space Sensor Technology and Planetary Exploration, Berlin, *Germany*,
[3]Geological Department, Brown University, Providence, RI, *USA*,
[4]Geological Department, Moscow State University, *Russia*,
[5]Max-Plank Institut fur Aeronomie, Katlenburg-Lindau, *Germany.*

Introduction: This work appeared as a result of analysis of the characteristics at the Mars Polar Lander landing site [1,2]. The latter was planned to be within polar layered deposits (PLD) composed of mixtures of ice and airborn dust [3]. Darker, less red (than PLD) material was observed there in topographic depressions and interpreted to be eolian deposit caught in the saltation traps [4]. Saltation implies sand size particles so the question arised how these particles could appear in the dust-and-ice environment. It was suggested by [1,2] that meteorite bombardment of PLD could partially transform their silicate dust component into the impact melt sand-sized particles, which became a source of the eolian deposits. To explore this possibility we simulated the impact melting of the Mars soil analog and measured reflectance spectra of the melting products. The failure of the Mars Polar Lander did not close the problem of contribution of the impact melt to the composition of Martian soils. Moreover it is evident that because meteorite bombardment affects Mars globally, the results of this study are applicable to much broader analysis of the spectra of this planet.

Martian soil analog: For our experiments we used JSC Mars-1 simulant (palagonite soil) [5]. The sub-sample studied by us is close in its chemistry to that described in [5] except LOI which is higher (21.8 wt %) in their and lower (15.88%) in our sub-sample. Our analysis showed that the dominant part of LOI is CO_2 (11.12%), H_2O is second in abundance (5.40%). S is <0.3%. N_2 is 0.058%.

Experiments: Melting associated with impacts reworking of regolith is fast and occurs with superheating of significant part of the melt [6,7]. Its products are typically dispersed and hence cool very fast. We simulated impact melting of palagonite at Vernadsky Institute producing glasses by: 1) fast melting in the resistance furnace at ~1650°C and fast (seconds, glass F) and more

#This study was partly supported (for ATB) by the Alexander von Humboldt Foundation.

slow (10's sec, glass S) cooling at vacuum ~10^{-1} mm Hg; and 2) by laser shots thus melting very fast small pieces of the target which cooled also very fast (<1sec), vacuum ~10^{-2} (glass L2) and ~10^{-4} mm Hg, (glass L4). Vacuum ~10^{-1} to ~10^{-2} mm Hg has oxygen fugacity close to that in Mars atmosphere [8].

Grains of fractions +200-380 μm of samples F, S, L2, L4, and P were sealed in epoxy, polished and then studied at Moscow State University Camscan 4 DV + Link AN10000. For most components the microprobe analyses did not show systematic compositional differences between the produced glasses and the palagonite sample and among the produced glasses except some depletion of L2 and L4 in Na and K.

The SEM study showed that glass S (Fig. 1, left) is compositionally homogeneous and looks massive with no gas bubbles. Glasse F (Fig. 1, right) shows compositional inhomogeneities seen as variations in the brightness on BSE images and sometimes has gas bubbles larger than 10-15 μm across. Sometimes clusters of very small (~1 μm) bright (on BSE images) grains of Fe-Ti oxides and skeletal crystals of plagioclase, olivine and ilmenite are seen included in the F glass.

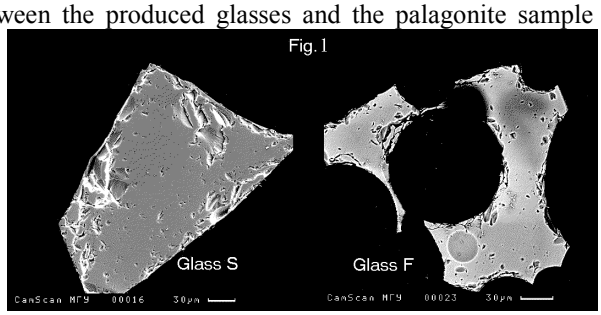

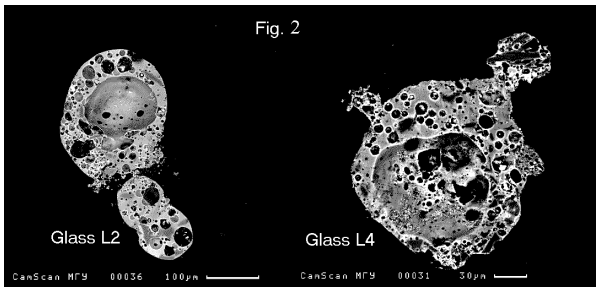

Glasses L2 and L4 (Fig. 2) are represented by spheroidal droplets and irregular fragments with numerous gas bubbles of 1-2 to 30-50 μm across. The glass in between bubbles frequently shows compositional inhomogeneities with typical size from a few microns to a few tens of microns. In rare cases inclusions of minerals such as plagioclase are observed.

Spectral measurements: The reflectance spectra of several size fractions of the samples were recorded between 0.3 and 25 μm at Brown University using spectrometers RELABbds and Nicolet 740 FTIR, and at DLR, Berlin, using spectrometer Bruker IFS88. Although the glasses show spectral variability depending on the method of production and the cooling rate [9] all of them are darker and less red relative to palagonite (P). Below is an example of the preliminary results: the 0.59/0.45 μm ratios:

Size, μm	P	S	F	L2	L4
200-380	2.33	~1.05	~1.05	1.73	~1.7
<40	3.06	1.58	1.42	2.02	2.11

Discussion and conclusions: It was found in [4] that dust mantling PLD has 0.59/0.45 μm ratios to be 3.2-3.7, while darker, less red material in topographic depressions has the ratios 1.8-2.1. It was suggested in [4] that the dark material consists of sand-sized particles which could form from the local dust, e.g., through aggregation of dust particles in the process of sublimation of the dusty ice [10,11]. However, the latter authors noted that color and brightness of the aggregates do not differ significantly from those of the dust. That is why [1,2] suggested that meteorite impacts into the layered deposits could produce the glass particles then involved in saltation and forming the darker and less red deposits in local lows. Spectral studies of our experimental glasses showed that they are indeed darker and less rede than the Martian soil simulant. This agrees well with the suggestion of [1,2]. We expect that future missions to Mars will identify impact melt glasses in the regolith of polar regions and in other areas of Mars and confirm their importance in forming the lithology of the surface layer of this planet.

Unexpected implications: Among other features detected in spectra of the experimental glasses, the 4.27-μm absorption was found [9]. Similar (4.25-μm) feature was recently described in NIMS spectra of Callisto and Ganymede and interpreted as signature of CO_2 trapped in interstitial spaces or fluid inclusions in water ice [12]. In our studies the 4.27-μm absorption was found only in the spectra of the L2 and L4 glasses [9]. The latter differ obviously from the F and S glasses in the presence of numerous gas bubbles (Figs 1 and 2). So one may suggest that this feature is a signature of CO_2 trapped in the observed bubbles and/or in some other form. This is supported by the fact that the dominant part of LOI of the used palagonite is CO_2. Laser shots are good simulation of high-velocity micrometeorite impacts. This implies that micrometeorite bombardment of targets, which release on their melting gas CO_2, may produce glass with CO_2 gas bubbles. Good candidates for such targets are 1) surface materials of the DPC asteroids and 2) compositionally close to them dark non-icy lag material on the surfaces of Callisto and Ganymede. If so: 1) we may suggest that the 4.25-μm absorption in spectra of these satellites is, at least partly, due to CO_2 trapped in the silicate glass produced by the micrometeorite bombardment; and 2) we may expect the 4.25-μm feature in spectra of DPC asteroids is also related to the gas release in micrometeorite bombardment of their regoliths.

References:

1. Basilevsky A. et al. (1999) *5th Intern. Conf. on Mars*, Abs. 6060.
2. Basilevsky A. et al. (1999) *Solar System Research,* 33, 438-448.
3. Thomas et al. (1992)) In *Mars*, H. Kieffer et al., eds. U. Arizona Press, 767-798.
4. Herkenfoff K. & Murray B. (1990) *JGR*, 95, 1343-1358.
5. Allen C. (1998) *LPS XXIX*, Abs. 1690.
6. Basilevsky A. et al. (1983) *Impact Craters on the Moon and Planets*, Moscow, Nauka.

7. Melosh H. (1989) *Impact Cratering. A Geologic Process*, Oxford U. Press.
8. Owen T. (1992) In *Mars*, H. Kieffer et al., eds. U. Arizona Press, 818-834.
9. Moroz L. et al. (2000) LPS XXXI, Abs. 1532
10. Saunders R. et al., (1986) Icarus, 66, 94-104.
11. Storrs A. et al., (1988) Icarus, 76, 493-512.
12. McCord T. et al. (1998) JGR, 103, 8603-8626.

Kuskov O.L. and Kronrod V.A. Models of chemical composition and internal structure of the Galilean satellites of Jupiter

Vernadsky Institute of Geochemistry and Analytical Chemistry RAS, Moscow ol_kuskov@mail.ru

key words [*Jupiter satellites composition*]

Being a smaller analogue of the solar system, the Jupiter system consists of 16 moons: the four Galilean moons - Io, Europa, Ganymede, and Callisto (in order of increasing distance from Jupiter) - and a number of smaller satellites. A direct study of the Galilean satellites, started by space probes of the Pioneer and Voyager series, was continued by the Galileo spacecraft. The data obtained on the gravitational fields of the satellites made it possible to determine the dimensionless moments of inertia for Io, Europa, and Ganymede and to estimate their core sizes. We consider here a five-layer model of the internal structure of a satellite, including a silicate crust or an ice layer, a three-layer mantle, and an Fe-FeS core. Solving the optimisation problem, we have used the separation of the mantle in order to estimate the ranges of the composition and density distribution in the mantle reservoirs and to find out the dependence of the core sizes on the densities. The chemical and phase compositions of the satellite's mantle were modeled within the system Na_2O-TiO_2-CaO-FeO-MgO-Al_2O_3-SiO_2 (NaTiCFMAS) including the solid solution phases: olivine, spinel, plagioclase, ilmenite, and garnet (almandine, grossular, pyrope); orthopyroxene and clinopyroxene are 5-6-component solutions. The core was modeled by the Fe-FeS system with the density of 8.1 g cm^{-3} for iron core and 5.15 g cm^{-3} for an eutectic Fe-FeS composition at P-T conditions in the center of the satellites. The equations of state of the high-pressure phases of ice are taken into account.

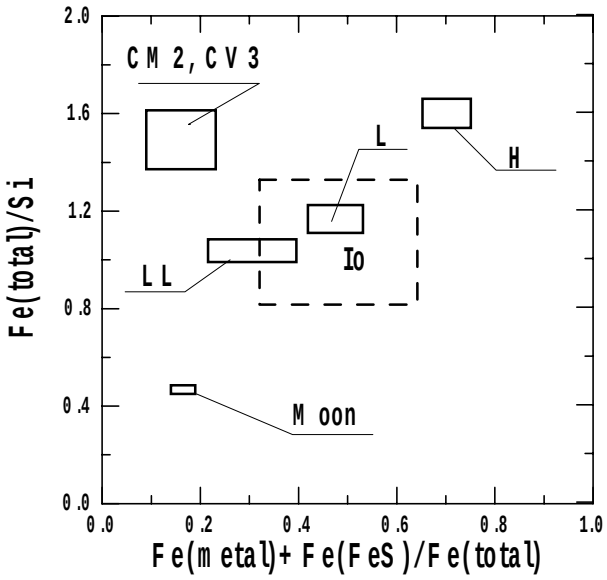

Fig. 1. Element weight ratios in Io derived from the geophysical constraints in comparison with those in chondrites. The ratios of $(Fe_{tot}/Si)^{Io}$=1.04-1.14 and $(Fe_m/Fe_{tot})^{Io}$ =0.37-0.5 calculated for bulk Io from silicate fraction of L and LL chondrites are in agreement with bulk elemental ratios for L and LL chondrites.

The densities in the mantle shells and core radii are found by the Monte-Carlo method [1,2]: the entire range of the geophysically and petrologically allowed mantle densities is examined and those values that obey the balance relations for the mass and moment within the uncertainty limit are chosen. The core sizes are evaluated from the conservation equation for the mass. For computation of the geophysically admissible density distribution models in the mantle layers and core radii, several million models were generated and tested. The successful models are analysed and are interpreted in terms of the bulk composition and internal structure of the satellites. The results are shown in Figs.1-3.

The correspondence between the density and moment of inertia values for bulk Io and rock-iron cores of Europa and Ganymede shows that their bulk compositions are, in general, similar and may be described by the composition close to L and LL chondrites. Geophysical and geochemical constraints show that H and carbonaceous chondritic materials may be excluded for the bulk compositions of these satellites. For L and LL chondritic composition and density models, radii of the Fe core and eutectic Fe-FeS core are estimated to be: R(Fe-core)=590-630 km and R(Fe-FeS-core)=830-875 km for Io; R(Fe-core)=420-490 km and R(Fe-FeS-core)=580-650 km for Europa; R(Fe-core)=610-710 km and R(Fe-FeS-core) = 820-900 km for Ganymede with an outer shell composed of the ice solid phases. If the Galilean satellites do have the L-, LL-chondritic composition, then their cores are probably Fe or Fe-rich, whereas large FeS cores are excluded by the composition of chondrites. The results of modeling support the hypothesis that Io, Europa and Ganymede have a massive metallic core in which a magnetic field may be produced.

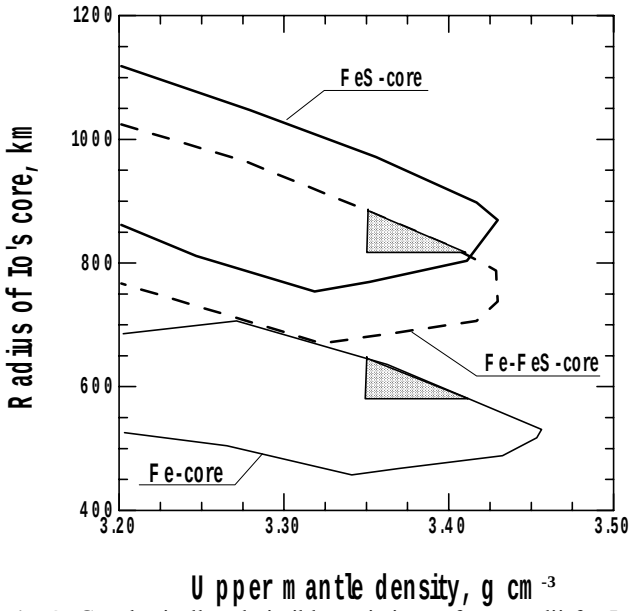

Fig. 2. Geophysically admissible variations of core radii for Io (H_{crust} =60 km and ρ =3.0 g cm^{-3}). The allowed core radii of Io vary from 440 to 720 km for an Fe core, from 640 to 1020 km for a eutectic Fe-FeS core, and from 750 to 1120 km for an FeS core. The silicate fraction of the L and LL chondrite composition assumed for the mantle yields core radii between 590 and 630 km for an Fe core, and between 830 and 875 km for a eutectic Fe-FeS core (shaded zone).

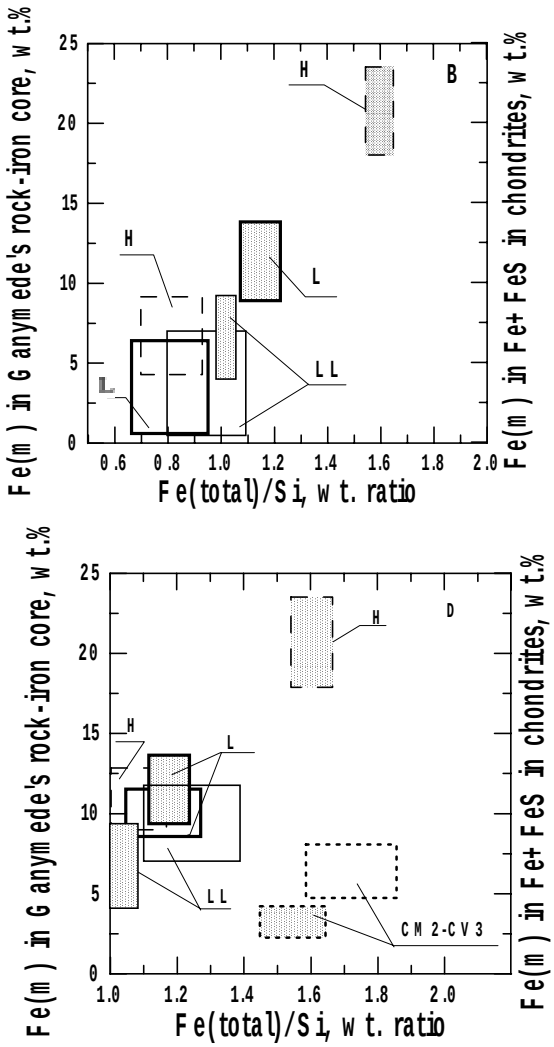

Fig. 3. Element weight ratios for chondritic models of Ganymede's rock-iron core (empty boxes) derived from the geophysical constraints in comparison with those in chondrites (shaded boxes). The empty boxes outline an allowed content of pure iron in a central Fe-core relative to the total rock-iron core mass. The density of the mantle is calculated from the silicate fraction of ordinary and carbonaceous chondrites. Model (D) - an outer shell is composed of solid ice phases. Model (B) - an outer shell with an inner liquid-water ocean (with the uppermost shell of ice-I 30-120 km thick).

For the L-, LL-chondritic composition of rock-iron cores, thickness of an ice-liquid outer shell in Europa is estimated to be 120-140 km (7-8% of total mass); thickness of a solid ice outer shell in Ganymede is expected to be 890-920 km. The content of H_2O in Ganymede's icy envelope is 46-48% of the total mass which is different from the cosmic mixture (~60% ice, 40% rock by mass).

Models, showing the outer shell of Ganymede to consist of a mixture of water and ice are considered, and thickness of the outer shell (750-840 km) and Fe-FeS-core radii are estimated. The possibility of an inner liquid-water layer beneath the icy surface of Ganymede can not be ruled out, if the bulk composition of its rock-iron core would be close to the composition of LL (rather than L) chondrites. In such a case, Ganymede's magnetic field may be associated with the existence of a metallic core as well as with a liquid-water ocean containing some electrolite.

References:

1. 1. Kuskov O.L.,Kronrod V.A.,1997. Models of internal structure of Io. Geokhimiya, 1171-1180.
2. 2. Kuskov O.L., Kronrod V.A.,1998. Models of internal structure of Jupiter's satellites (Ganymede, Europa and Callisto). Astronom. Vestnik, 32 (1) 49-57.

#Dorofeeva V.A.*, Makalkin A.B.** Fractionation of the protomaterial of the galilean satellites in the cooling dense circum-jovian disk

*Vernadsky Institute of Geochemistry and Analytical Chemistry RAS, Moscow
**United Institute of Phisics of the Earth RAS, Moscow

Recently we have calculated models of the protosatellite accretion disk around Jupiter in the late phase of its formation that is characterized by a relatively slow accretion onto the planet. In this phase the mass flux onto Jupiter decreased to 10^{-6} -10^{-7} M_J /year, and the Jupiter's luminosity lowered from the maximum values, but still remained high, approximately 1000 times higher than the modern one. We calculated distributions of temperature and pressure as well as positions of evaporation-condensation fronts for the water ice and magnesium silicates. The constraints placed on the disk models are the mass of the Galilean satellites and their chemical composition: the absence of water in Io, the low water content in Europe, and the high water content in Ganymede and Callisto. We found out that it is impossible

This work was supported by RFBR grant 98-05-64943.

to construct the model of the accretion circum-Jovian disk, which would simultaneously meet the compositional and mass constraints. Two types of models were constructed: (1) a low-mass, moderately warm, viscous disk, which satisfies the compositional constraint, and (2) three and a half orders more massive and less viscous disk constrained by mass, but substantially more hot that it is necessary for water ice condensation even in the formation zone of Callisto, the outermost of the Galilean satellites [1].

We considered consequences of either of the two disk models for the process of satellite formation. It was found that the low-mass model (1) runs into the problem to accumulate in the disk the mass of solid material, which is sufficient to form the regular satellites. A very high, almost 100%, efficiency of sweeping up the dust particles and small bodies by the satellite embryos over the whole period of their growth is required for the satellite formation, that is highly improbable. For accumulation of satellites from the low-mass disk it is also necessary that the intensive accretion of gas-dust material onto the disk and through it onto Jupiter continued no less than 1×10^7 years, that is, approached the lifetime of the gas in the solar nebula (the protoplanetary disk). However, it is much more probable, that the accretion rate decreased with time. In this case the mass of the solid component of the material arrived at the jovian disk appears to be insufficient to form the satellites.

In the massive disk model (2) such problems do not arise. In this model the matter falling on the disk from the solar nebula, at the early stage of disk evolution is accumulating in it due to its relatively low viscosity and, accordingly, lower radial mass flux through the disk. At this stage the disk temperature is growing. After completing the stage of accumulation of matter the quasi-stationary state is reached in the disk, the temperature of the inner region being higher than necessary to form the satellites of observed density and composition. However, then, as the mass flux on the disk and through it on Jupiter reduces, the temperature in the disk decreases concurrently with decrease of its mass and surface density. It is also possible, that the disk at the late stage of its evolution ceases to be accretion disk, that is, the turbulence is damped out and the viscosity tends to zero. As viscous dissipation decreases, the temperature in the disk is also lowered. In the case that the disk viscosity decreased faster than the mass flux falling on the disk from the surrounding solar nebula, the disk mass could grow till the end of the fall. The loss of the gas from the disk was carried out by the process of thermal dissipation. From our estimates it follows that the rate of this process was lower than the cooling rate of the disk and the growth rate of planetesimals in the inner zone of the disk, at the radial distances of the Galilean satellites (excluding Callisto).

Duration of formation of the satellites is defined not only by their accumulation rate which is proportional to the surface density σ_c of the solid (dust) component of the disk material. For the massive disk, corresponding to the model (2), the value σ_c is three and a half orders of magnitude higher, than for the model (1).

In view of the above considerations we choose the variant of formation of the Galilean satellites, based on the model (2) of the accretion Jovian disk. According to this model, at the steady-state stage of disk evolution (prior to the accumulation of the satellites) the disk was dense and hot. The process of satellite formation occurred at the subsequent stage of disk cooling due to decaying accretion on Jupiter. The temperatures and pressures in the mid-plane of the disk at several successive moments from the beginning till the end of this stage are shown in Fig.1. One can see that the pressures at the radial distances corresponding to the region inside of Ganymede orbit ($r < 15r_j$), were for a long period ($\geq10^5$ years) higher than 0.01 bar. This suggests that the temperatures inside the disk of solar composition at these radial distances were equal to the condensation temperature of iron-nickel alloy and higher then the condensation temperature of the major magnesium silicates. The difference between these temperatures, according to the calculations of the homogeneous condensation of the solar-composition gas, grows with the increasing total pressure and reaches 100 K at P = 0.1 bar and 150 K at P = 1 bar [2]. The disk structure just before the cooling stage, obtained from our modeling, is shown in Fig.2. The innermost, rather extended region of the disk ($r < 17r_j$) is a region of partial condensation of the metal, bounded by the front of the total metal condensation (curve z_{Fe}). The condensation front of Mg-silicates is located outside the metal condensation front at the distance $\leq 1\ r_j$ from the latter. The region of partial condensation of Fe-Ni alloy contained also in the solid state Al, Ca and other less abundant refractory elements. The reason why the Fe-Ni in the inner region of the disk was not evaporated totally, is the following. The disk was heated from the interior due to the dissipation of turbulence (viscous dissipation); the energy transfer from the interior to the subsurface layers of the disk was carried out by radiation, and the heat flux depended on the opacity of the disk material. As Mg-silicates in the inner region were evaporated, the opacity there was dictated by the most abundant metal particles. The heating of this region above the condensation temperature of Fe-Ni alloy and its total evaporation would produce a sharp drop of opacity, an increase of the energy flux from the interior layers, and hence a decrease of their temperature and partial condensation of the metal.

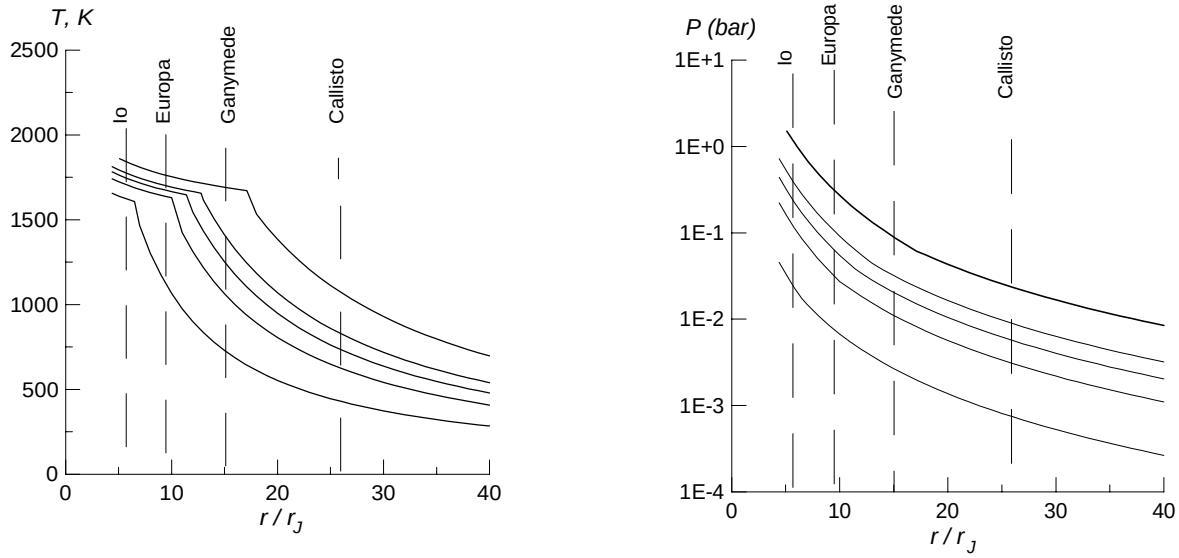

Fig.1. Radial distribution of the temperature and pressure at several successive moments of the stage of disk cooling and formation of the Galilean satellites. The radial coordinate is given in the units of the present mean radius of Jupiter.

At high temperatures iron particles grow rapidly at collisions due to their high plasticity [3]. In conditions of circum-Jovian disk at the distance $r = 10r_J$ they reached the size 1 cm in 10^3 years. As it follows from our estimates, a decrease of orbital radii of the particles due to gas drag resulted in their fall on Jupiter in a time of the same order. The gas drag is caused by the difference between the orbital velocities of the particles and gas: the gas velocity is lower due to existence of the radial gradient of gas pressure in the disk. The time of settling (precipitation) of the particles to the midplane of the disk with regard to disk's turbulence at $r = 10r_J$ is estimated as $\geq 10^3$ years. This means that iron particles before their fall on Jupiter had no time to form in the midplane the gravitationally unstable dust layer, necessary for formation of large planetesimals, those could not be removed from the disk and carried to Jupiter.

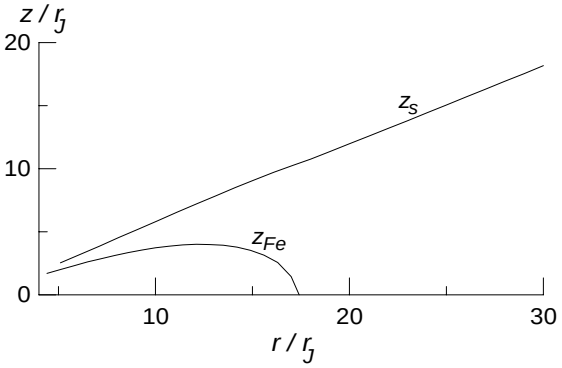

Fig.2. Meridional section of the protosatellite circum-Jovian disk at the stage prior to disk cooling. Curves z_s and z_{Fe} are the optical surface of the disk and the metal condensation front. All heights are measured from the midplane of the disk.

The gas drag continuously supplied new portions of dust particles from the outer to the inner zone of the disk. These particles contained Fe, Mg and Si in the solar proportion. On arrival in the inner zone, Mg and Si evaporated, and the Fe-Ni particles (containing also more refractory elements) drifted to Jupiter due to gas drag. Hence, during a considerable period (10^5-10^6 years) of the high-temperature stage, there happened a depletion of the proto-satellite matelial in Fe. At the later stage the mass of the disk substantially decreased, the temperatures became lower, and the major mass of the rock-forming elements condensed in the zone of formation of the inner Galilean satellites - Io and Europe. However, due to preceding fractionation, the condensate was depleted in iron and more refractory elements. This conclusion agrees with the models of the internal structure of Io and Europe, based on evidence from new measurements of physical parameters of these satellites [4].

References:

1. Makalkin A.B., Dorofeeva V.A., Ruskol E.L. Modeling the protosatellite circum-Jovian accretion disk: an estimate of the basic parameters. *Solar System Research*, 1999, 33, no.6, pp.456-463.
2. Saxena S.K., Erikson G. Chemistry of the formation of the terrestrial planets. In *Chemistry and physics of terrestrial planets*, Saxena, S.K., Ed., Berlin: Springer, 1986. pp.30-105.
3. Makalkin A.B. Possibility of formation of an originally inhomogeneous Earth. *Phys.Earth Planet.Inter*. 1980, vol.22, no.3, pp.302-312.
4. Kuskov O.L., Kronrod V.A. Models of chemical composition and internal structure of the galilean satellites of Jupiter (this volume).